

Experimental assessment of thermal break strips performance in load-bearing and non-load-bearing LSF walls

Paulo Santos* and Diogo Mateus

ISISE, Department of Civil Engineering, University of Coimbra, Pólo II, Rua Luís Reis Santos, 3030-788 Coimbra, Portugal

* Correspondent author: Paulo Santos, pfsantos@dec.uc.pt

A B S T R A C T

A reliable evaluation of thermal behaviour and energy efficiency of buildings depends on the accurate thermal characterization of the envelope components. One of the most reliable methodologies to perform this thermal characterization is the measurements under laboratory-controlled conditions. The thermal performance assessment of lightweight steel-framed (LSF) building components exhibits particular additional challenges related to the strong thermal conductivity contrast between cavity insulation and steel frame materials, which may originate unwanted significant thermal bridge effects. The use of thermal break (TB) strips is one of the most currently used thermal bridge mitigation strategies. It was not found in the literature any experimental campaign for TB strips thermal performance evaluation in LSF elements. In this paper the thermal performance of twenty load-bearing (LB) and non-load-bearing (NLB) LSF walls configurations are measured, using the heat flow meter (HFM) method under controlled laboratory conditions. Three thermal break (TB) strip materials and three TB strip locations in the steel stud flanges are assessed. It was found that the inner and outer TB strips show very similar thermal performances, while double TB strips have a relative significant thermal performance increase. Aerogel was the best performance TB material, exhibiting a substantial improvement relatively to recycled rubber and cork/rubber composite TB strips. Furthermore, the TB strips performance was identical for the evaluated structural (LB) and non-structural (NLB) LSF walls.

Keywords: Lightweight steel frame, LSF walls, Load-bearing, Non-load-bearing, Thermal resistance, Thermal break strips, Experimental measurements.

1. Introduction

A reliable and accurate thermal characterization of building envelope components is very important at design stage to predict future thermal behaviour and energy efficiency, as well as in existing buildings for energy audits [1]. Several thermal performance assessment methods are available nowadays, such as the use of catalogues [2] [3], analytical calculations [4] [5], numerical simulations [6] [7] and measurements (*in situ* or under controlled laboratory conditions) [8] [9].

The use of catalogues is limited to the existing component configurations in the provided database, which oftentimes could not be enough. The use of standard analytical methods such as the ones prescribed by ISO 6946 [5] are limited to building components with homogeneous and/or inhomogeneous layers, being the level of heterogeneity restricted. In fact, the ISO 6946 Combined Method [5] is not applicable to building components where the thermal insulation is bridged by metal, such as happens frequently in lightweight steel frame (LSF) elements.

In fact, given the huge thermal conductivity contrast between the steel frame and the batt thermal insulation materials, there is a strong thermal bridge effect, being harder to accurately evaluate the overall thermal resistance (or transmittance) of these type of building elements [10]. There are several analytical methods developed specifically for LSF building components, such as the Gorgolewski methods [11], the ASHRAE Zone Method [10] and ASHRAE Modified Zone Method [12]. Santos *et al.* [4] recently performed a calculation procedures review and accuracy comparison of these analytical methods to estimate the thermal transmittance of LSF walls.

With the increasing computer speed and calculation capacity, the heat transfer numerical models had become more detailed and accurate. These numerical simulations could be simpler two-dimensional (2D) models [6] [13] or more complex/detailed three-

dimensional (3D) models [14] [15], allowing a quick comparison between several building component configurations. However, to be fully reliable these simulations need to be validated against measured data or at least verified by comparison with benchmark results.

In fact, none of the previously mentioned thermal performance assessment methods fully replace the measurements under controlled laboratory conditions or *in situ*, having each method some advantages and/or limitations [8]. As recently reviewed by Soares *et al.* [8], there are several measurement methods for thermal characterization of building elements, including: (1) Heat flow meter (HFM) method [9] [16] [17] [18]; (2) Guarded hot plate (GHP) method [19]; (3) Hot box (HB) method [20], which could be calibrated (CHB) or guarded (GHB), and; (4) Infrared thermography (IRT) method [21].

The HFM method is one of the most used experimental technique for *in situ* assessment of thermal performance of building components, being attracting the researcher's attention in order to minimize his usual long duration [22] [23], evaluate uncertainty [24], compare with other methods [25] and increase precision [22]. It was concluded that the local operative conditions (*e.g.* high temperature gradient variation and heat flow inversion) can significantly influence the obtained *in situ* thermal transmittance [24]. Thus, whenever possible the HFM measurements should be performed under controlled temperature conditions (*e.g.* in laboratory). Moreover, it was found that the use of an additional heat flux sensor can significantly reduce test duration and increase precision [22].

As mentioned before, besides all these measurement inherent issues, LSF building components exhibits a particular additional challenge related with the strong thermal conductivity inhomogeneity of cavity insulation and steel frame materials [26]. This issue also addressed the attention of researchers by comparing several methods to evaluate thermal performance of LSF elements [27] and even developing new assessment methods

for *in situ* measurements [28], as well as the evaluation of lateral heat transmission or flanking thermal losses [14].

Another LSF elements thermal performance research trend is the development, evaluation and comparison between thermal bridges mitigation strategies. This assessment could be performed making use of two- [6] or three-dimensional parametric studies [15]. Besides the use of slotted steel studs [29] (which have the major drawback of reducing the mechanical resistance of load-bearing LSF walls), the use of thermal break (TB) strips is one of the most used strategy to mitigate the steel studs thermal bridge effect [1], being this the main focus of research project Tyre4BuildIns – “*Recycled tyre rubber resin-bonded for building insulation systems towards energy efficiency*” [30]. Nowadays, there are available in the market several TB strip materials, which were specifically developed for this purpose (*e.g.*, aerogel TB strips from SpaceTherm®) or could be easily adapted for this use (*e.g.*, recycled rubber MS-R1 from AmorimCorkComposites® and cork/rubber composite MS-R0 from AmorimCorkComposites®).

It was not found in the literature any systematic experimental campaign for the evaluation of different TB strip materials, neither for the assessment of the best performance positioning for these TB strips (inner or outer steel flanges), nor to evaluate if the TB strips are more efficient in load- or non-load-bearing LSF walls, being all these features the major novelties of this study.

In this work, the overall surface-to-surface thermal resistance (R -value) of twenty different configurations of load- and non-load-bearing partition walls are measured in controlled laboratory conditions, to evaluate the thermal break (TB) strips performance for the mitigation of the thermal bridges originated by the steel studs. Three tests are performed for each wall, with the sensors at different high locations (top, middle and bottom) within the LSF wall test-sample surfaces, totalizing sixty lab tests. Three TB strip materials are

tested, namely: (1) recycled rubber MS-R1; (2) cork and rubber composite MS-R0, and; (3) aerogel CBS. Three different TB strip positions within the steel stud flange are tested: (1) inner; (2) outer, and; (3) two TB strips.

The paper is structured as follows. After this brief introduction, the related materials and methods are presented, including LSF characterization, experimental lab tests and numerical simulations. Then, the obtained results regarding the overall surface-to-surface *R*-values, the infrared surface images and horizontal surface temperature lines are presented and discussed for the assessed structural and non-structural LSF partition walls. Finally, the main conclusions from this research work are summarized.

2. Materials and methods

2.1. LSF Walls Characterization

In this section the load- and non-load-bearing LSF walls, as well as the thermal break (TB) strips are characterized regarding materials, geometries/dimensions and thermal properties.

2.1.1. Non-load-bearing reference LSF wall

Figure 1 illustrates the cross-section of the reference non-load-bearing (NLB) LSF wall. The vertical steel studs (C90×37×15×0.6 mm) are spaced 400 mm apart and the steel sheet is 0.6 mm thick. The 90 mm cavity is full-filled with mineral wool (MW) batt insulation. The outer and inner sheathing surfaces are constituted by two gypsum plasterboards (GPB) on each side (2×12.5 mm thick), being this LSF wall perfectly symmetrical regarding a central vertical plane.

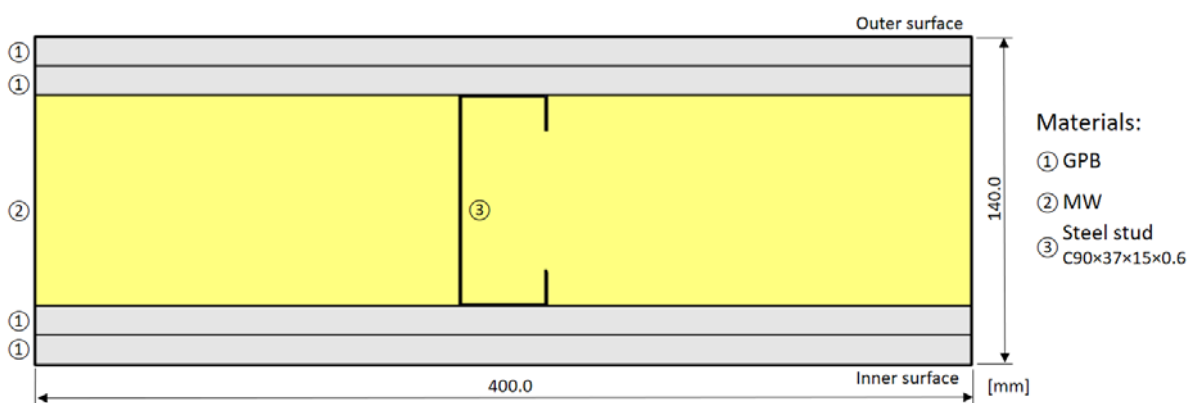


Figure 1. Reference non-load-bearing LSF wall horizontal cross-section: materials and geometry.

Table 1 displays the thickness of each wall layer, as well as the thermal conductivities of the materials. This NLB reference LSF wall has a total thickness equal to 140 mm.

Table 1. Reference non-load-bearing LSF wall material thickness (d) and thermal conductivities (λ).

Material (from outer to innermost layer)	d [mm]	λ [W/(m·K)]	Ref.
GPB ¹ (2 × 12.5 mm)	25.0	0.175	[6]
MW ²	90.0	0.035	[6]
Steel stud (C90 × 37 × 15 × 0.6 mm)	---	50.000	[3]
GPB ¹ (2 × 12.5 mm)	25.0	0.175	[6]
Total Thickness	140.0	---	---

¹GPB – Gypsum Plaster Board (Standard A: Gypted Iberica®); ²MW – Mineral Wool (AlphaRolo: Volcalis®).

2.1.2. Load-bearing reference LSF wall

The cross-section of the reference load-bearing (LB) LSF wall is illustrated in Figure 2, while the thickness of each wall layer and the thermal conductivities of the materials used are listed in Table 2. Being a load-bearing wall, the steel studs (C90×43×15×1.5 mm) are thicker (1.5 mm instead of 0.6 mm), but the spacing between vertical studs are kept the same as for the NLB reference LSF wall (400 mm). The MW batt insulation is also the same (90 mm thick). On each side of the steel studs there is an OSB structural sheathing panel (12 mm thick). In the inner surface there is an additional GPB sheathing layer (12.5 mm). The total thickness of this LB reference LSF wall is 126.5 mm.

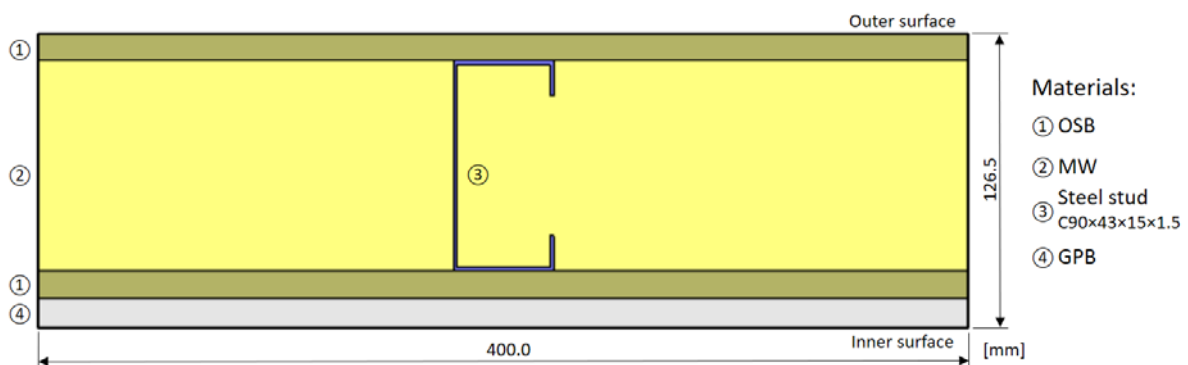


Figure 2. Reference load-bearing LSF wall horizontal cross-section: materials and geometry.

Table 2. Reference load-bearing LSF wall material thickness (d) and thermal conductivities (λ).

Material (from outer to innermost layer)	d [mm]	λ [W/(m·K)]	Ref.
OSB ¹	12.0	0.100	[6]
MW ²	90.0	0.035	[6]
Steel studs (C90×43×15×1.5 mm)	---	50.000	[3]
OSB ¹	12.0	0.100	[6]
GPB ³	12.5	0.175	[6]
Total Thickness	126.5	---	---

¹OSB - Oriented Strand Board (OSB3: KronoSpan®); ²MW - Mineral Wool (AlphaRolo: Volcalis®); ³GPB - Gypsum Plaster Board (Standard A: GyptecIberica®).

2.1.3. Thermal break strips

The thermal break (TB) strips used are 50 mm wide and 10 mm thick. As illustrated in Figure 3, the TB strips were placed along the inner, outer and both steel stud flanges. Three different materials were used in the TB strips: recycled rubber (MS-R1), recycled rubber and cork composite (MS-R0), and aerogel (AG), with decreasing thermal conductivities as illustrated in Table 3, ranging from 0.122 W/(m·K) down to 0.015 W/(m·K).

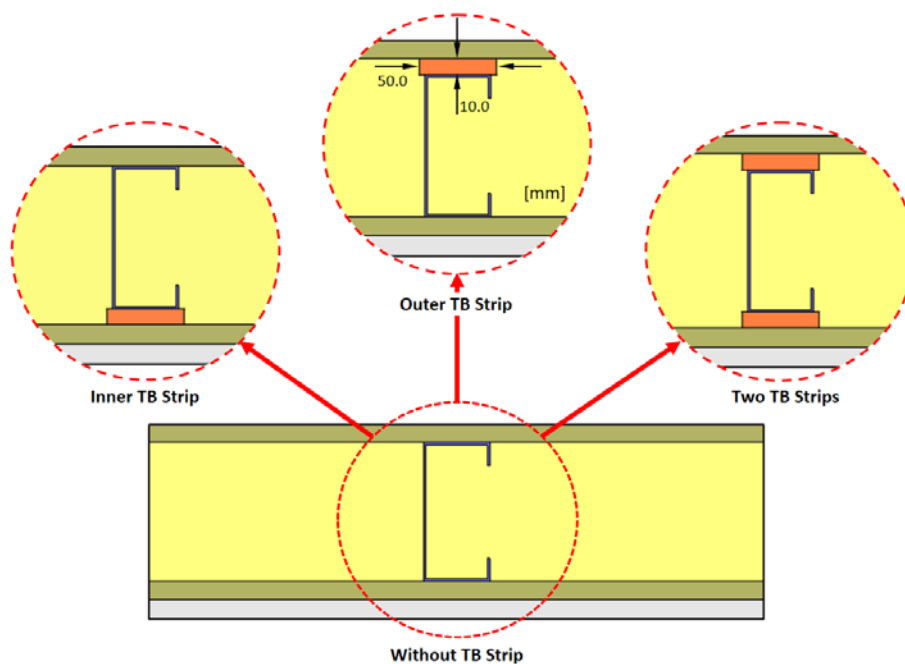


Figure 3. Geometry and location of the thermal break (TB) strips.

Table 3. Material and thermal conductivity (λ) of the thermal break strips.

Material	λ [W/(m·K)]	Ref.
Recycled rubber (MS-R1)	0.122	[6]
Recycled rubber and cork (MS-R0)	0.088	[31]
CBS ¹ Aerogel (AG)	0.015	[6]

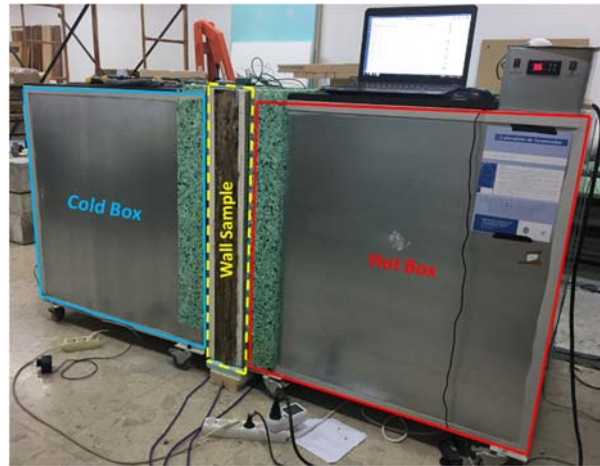
¹CBS – Cold Break Strip.

2.2. Experimental Lab Tests

2.2.1. Experimental setup

The laboratorial tests were performed using a mini hot box apparatus, as illustrated in Figure 4a, which was used as a set of two climatic chambers, being the thermal performance of the LSF walls measured using the heat flow meter (HF) method [9] adapted to have two HF sensors [8]. The cold box is cooled by a refrigerator Electrolux® (Model ERT 6658) attached to it (Figure 4b), while the hot box is heated by an electrical resistance (70 watts), as shown in Figure 4c. These two climatic boxes are well insulated by a 140 mm thick XPS layer, minimizing surrounding heat losses and ensuring a quasi-steady-state temperature difference between the two surfaces of the LSF test sample (Figure 4a).

To promote air circulation, mitigating air temperature stratification inside hot and cold boxes, two small fans (12V, 0.15A) were used as illustrated in Figure 5a. Moreover, a black radiation shield was placed near the wall sample (10 cm apart), one inside the hot box and another one inside the cold box (Figure 5b). To allow an interior air flow near the wall being tested, these baffle plates have a 5 cm gap around his perimeter.



a) Cold and hot boxes with the wall sample



b) Refrigerator attached to the cold box



c) Electrical resistance inside hot box

Figure 4. Mini hot box apparatus used in the experiments.

The LSF wall test samples used in these measurements have 1030 mm height and 1060 mm width, having three vertical steel studs, being the middle one centred, as illustrated in Figure 6a. Notice that to minimize the heat losses through the lateral surfaces of the LSF wall sample, its perimeter was covered by 80 mm of polyurethane foam insulation (not illustrated), having this foam material a thermal conductivity equal to 0.036 W/(m·K).

As suggested by Rasooli and Itard [22], besides the heat flux meters (HFMs) placed in the hot side, they were also placed in the cold side of the LSF wall sample, increasing the accuracy of the measurements and reducing his duration. Therefore, four HFMs (Hukseflux model HFP01, precision: $\pm 3\%$) were used, being half on the hot surface and the remaining ones on the cold wall surface. In both wall surfaces (hot and cold) one HFM was located in the vicinity of the vertical steel stud (HFM1) and another one in the middle of

the insulation cavity (HFM2), as illustrated in Figure 6b, allowing to measure the two distinct thermal behaviour zones within the LSF wall sample.

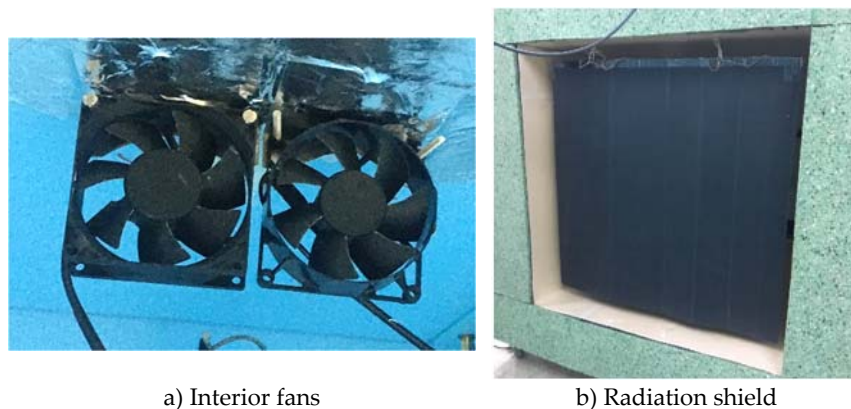


Figure 5. Mini hot box equipment details.

Temperatures were measured using type K (1/0.315) PFA insulated thermocouples (TCs), certified with class 1 precision. Moreover, each one of the twelve TCs used in the measurements was calibrated in the temperature range [5°C; 45°C], with a 5°C increment, making use of a thermostatic stirring water bath (Heto CB 208), where the TCs were immersed. The record interval was 10 seconds for a measurement duration of 5 minutes for each calibration temperature. The calibration equation for each TC was found making use of a linear trend line along the 9 calibration temperatures.

Half of the TCs were used for the measurements in the hot side of the tested wall, while another half (six) were used in the cold side. Among these six cold or hot TCs, two measured the environment air temperature inside each box (TC5 and TC6), another two measured the air temperature between the radiation shield and the wall surface (TC3 and TC4), while the remaining two measured the wall surface temperatures (TC1 and TC2), as illustrated in Figure 6b.

The temperature and heat flux data measured during the experiments were recorded making use of 2 PICO TC-08 data-loggers (precision: $\pm 0.5^\circ\text{C}$), one for each side of the LSF wall test-specimen (hot and cold). These data-loggers were connected to a laptop and the software used to manage this data was the PicoLog version 6.1.10.

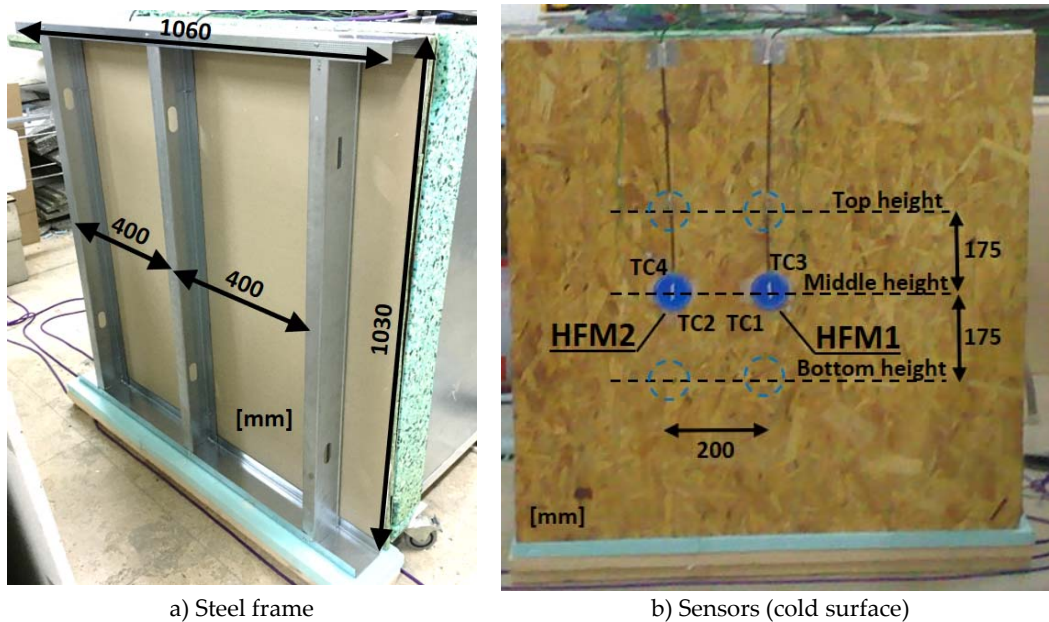


Figure 6. Tested LSF wall sample (TC-Thermocouple; HFM-Heat flux meter).

2.2.2. Set-points and test procedures

The test procedures used in this work to measure the LSF walls thermal performance (surface-to-surface R -value) were based on some of the prescriptions provided by several international standards, namely ISO 9869-1 [9], ASTM C 1155-95 [18] and ASTM C 1046-95 [17]. The standard ISO 9869-1 [9] prescribe the “average method” to evaluate the R -value of a building element, which has strong similarities with the “summation technique” prescribed in the American standard ASTM C 1155-95 [18].

Notice that, to avoid additional uncertainties and to allow the posterior computation of the total thermal resistance (R -value) or transmittance (U -value) for several indoor-outdoor temperature conditions and corresponding film coefficients, the thermal performance of the assessed LSF walls is evaluated based in the obtained conductive or surface-to-surface global thermal resistances.

As mentioned before, in these experiments it was used the heat flow meter (HFM) method [9], but with an improvement, as suggested by Rasooli and Itard [22], to increase precision and reduce test duration. The improvement consists of measuring heat fluxes simultaneously at both hot and cold wall surfaces, instead of measuring in only one side, as

prescribed by ISO 9869-1 [9].

The measurements were performed in a quasi-steady-state heat transfer condition and the temperature set-points provided for the hot and cold boxes were 40°C and 5°C, respectively. This warmer set-point temperature (40°C) is higher than the usual indoor winter comfort temperature (*e.g.*, 18°C or 20°C) in order to increase the temperature gradient between both surfaces of the test sample wall, increasing reliability and accuracy of the measured R -values [9]. The data measured by all the sensors were recorded every 10 seconds and the computations to obtain the local conductive R -value, for each test, were later performed making use of average hourly values.

In this work it was adopted the convergence criteria prescribed in ASTM C1155–95 [18] for the “summation technique”, *i.e.*, assuming a maximum admissible convergence factor equal to 10%. Therefore, only the estimated hourly R -values having an absolute difference, in relation to the previous time obtained R -value, lower than 10% were considered in the measurements. The minimum duration of each measurement test was 24 hours.

To ensure the repeatability of the experimental measurements, one test was performed for each wall at three height locations, as illustrated in Figure 6b, that is: (1) top, (2) middle, and (3) bottom, being the average of these three tests the considered measured overall conductive R -value of the LSF wall.

Making use of the data recorded (heat fluxes and temperatures) for each test and applying the HFM method [9], two distinct conductive local R -values were obtained: (1) a lower value for location 1 (Figure 6), *i.e.*, in the vicinity of the steel studs (R_{stud}), and; (2) a higher value between the steel studs, *i.e.*, in the middle of the insulation cavity (R_{cav}). The overall surface-to-surface R -value of the wall (R_{global}) was obtained by computing an area weighted of both measured conductive R -values, as indicated in the following equation,

$$\frac{1}{R_{global}} = \frac{1}{R_{stud}} \frac{A_{stud}}{A_{global}} + \frac{1}{R_{cav}} \frac{A_{cav}}{A_{global}}, \quad (1)$$

where A_{global} is the total area of the LSF wall [m^2], A_{stud} is the area of influence of the steel stud [m^2] and A_{cav} is the remaining cavity area of the LSF wall [m^2].

The steel stud influence area (A_{stud}) was defined as prescribed by ASHRAE zone method [12], *i.e.*, assuming a zone factor (zf) equal to 2.0 [4]. Therefore, the width of the steel stud influence zone (w) is equal to the flange length (fl) plus two times the thickness of the thicker sheathing layer ($d_{thicker}$).

Notice that these computations to obtain an overall R -value of the tested LSF wall were performed making use of a representative wall zone area defined by the studs spacing (width) and assuming one meter high (length), *i.e.*, 0.40 m by 1.00 m (0.40 m^2).

2.2.3. Experimental procedures verification

To verify the good working conditions and reliability of the implemented experimental apparatus (*e.g.* sensors and data-loggers) previously described, it was decided to test, under the same conditions, a homogeneous XPS panel (Topox® Cuber SL) with 60 mm thick, having a known thermal conductivity: 0.034 W/($m \cdot K$). The measured surface-to-surface thermal resistance was 1.784 $m^2 \cdot K/W$, which allowed to obtain a corresponding thermal conductivity equal to 0.034 W/($m \cdot K$), *i.e.* the same value provided by the XPS manufacturer.

Besides the previous verification making use of a homogeneous XPS panel, all the LSF wall measurements results (overall conductive R -values) were compared with bi-dimensional finite element numerical simulations, as detailed in the following Section 2.3. The obtained results for non-load-bearing (Table 4) and load-bearing LSF walls (Table 5), showed and discussed later in paper (see Section 3), exhibits a very good agreement, between lab measurements and numerical simulations, having a maximum error/difference

equal to $\pm 3\%$.

2.3. Numerical Simulations

The finite element method (FEM) software THERM® (version 7.6.1) was used to perform the 2D numerical simulations of the LSF walls. The corresponding model details are explained next.

2.3.1. Domain discretization

Being a bi-dimensional FEM numerical simulation, only a 2D representative part of the walls cross-sections (400 mm width) was modelled, as previously illustrated in Figure 1 and Figure 2, for the reference non-load and load-bearing LSF walls, respectively. The thermal properties of the materials used in these simulations were previously presented in Section 2.1 (tables 1, 2 and 3). Moreover, the maximum error admitted on the FEM computations was set to 2% for all models built and assessed in this work.

2.3.2. Boundary conditions

Two sets of boundary conditions are needed to be defined for each THERM model: environment air temperatures and surface thermal resistances. The warmer “internal” and colder “external” air temperatures were set equal to the set-points defined for hot and cold climatic boxes in lab measurements, *i.e.* 40°C and 5°C, respectively (see Section 2.2.2). Notice, that the obtained R -values do not depend on the chosen temperature difference between the interior and exterior environments, since these values are computed for a unitary temperature difference.

The surface thermal resistances were modelled using the average values measured for each test and for each LSF wall surface, taking into account the air and surface temperature differences and the surface heat fluxes. The measured surface thermal resistances, ranging within the interval $[0.08; 0.13] \text{ m}^2\cdot\text{K}/\text{W}$, were within the range defined

in ISO 6946 [5] for horizontal heat flow, *i.e.*, between $0.04 \text{ m}^2\cdot\text{K}/\text{W}$ for external surface resistance (R_{se}) and $0.13 \text{ m}^2\cdot\text{K}/\text{W}$ for internal surface resistance (R_{si}), being closer to this last value.

Notice that, as mentioned and justified before, in this work only are used conductive (or surface-to-surface) R -values to analyse the thermal performance of the LSF walls, *i.e.* the surface thermal resistances are not included. Nevertheless, they need to be defined in the THERM models, making use of a film coefficient ($1/R_s$), being afterward subtracted.

2.3.3. Accuracy verifications

To ensure a good accuracy of the THERM models several verifications were made, namely: (1) ISO 10211 [7] test cases verification; (2) Homogeneous wall layers verification, and; (3) Experimental lab measurements validation.

Regarding the two bi-dimensional test cases prescribed by standard ISO 10211 [7], the heat transfer FEM algorithm of the THERM software is classified as a steady-state high precision algorithm. Moreover, the authors have a large experience using this software [27] [6] [4], having also performed these two standard test cases with success (not illustrated here).

The homogeneous wall layers verification consisted in modelling the two reference LSF walls, previously illustrated in Figure 1 (non-load-bearing) and Figure 2 (load-bearing), without the C-shape cold-formed steel stud and assuming the remaining wall layers as continuous and homogenous. This way, the analytical solution is known and could be applied for these two simplified models, being the total thermal resistance calculated as a sum of the layer's thermal resistances, as prescribed by ISO 6946 [5]. The obtained results are displayed in Figure 7, where both THERM and analytic R -values are exactly the same when assuming homogeneous layers for non-load ($2.857 \text{ m}^2\cdot\text{K}/\text{W}$) and load-bearing walls ($2.883 \text{ m}^2\cdot\text{K}/\text{W}$) reference configurations.

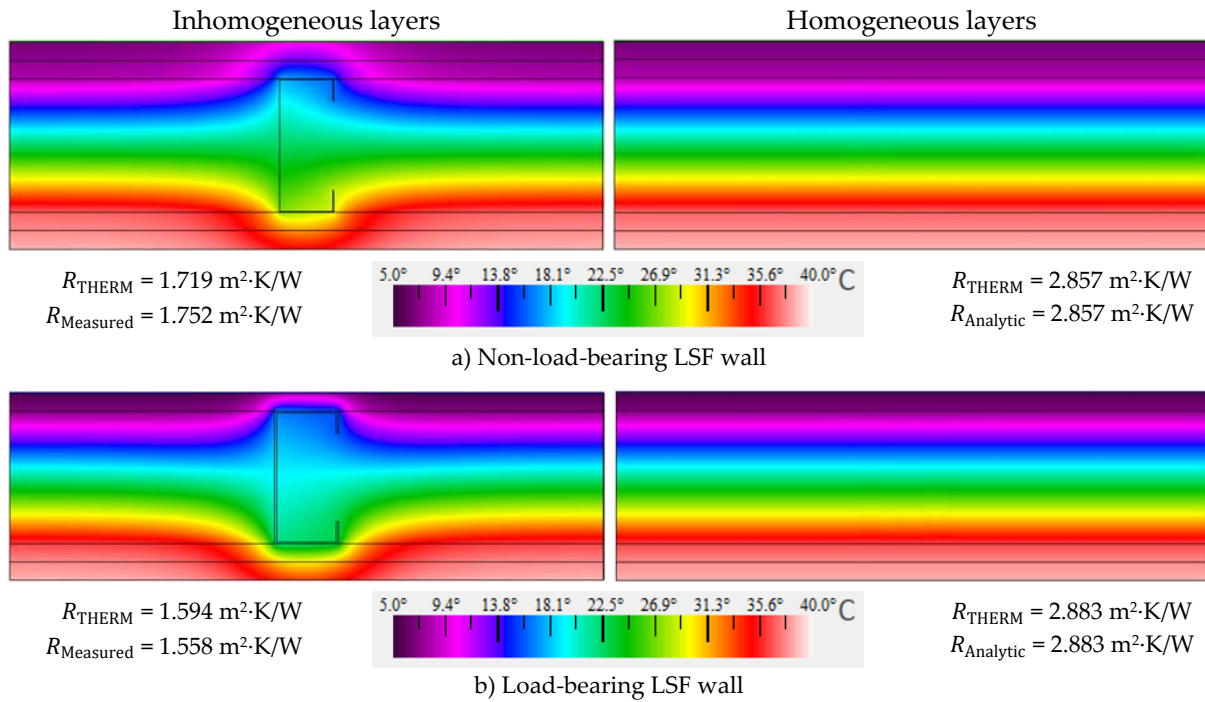


Figure 7. Accuracy verification of the THERM models: Temperature distribution and conductive R -values.

Regarding the lab measurements verification, Figure 7 also displays the measured overall surface-to-surface R -values of both load-bearing (LB) and non-load-bearing (NLB) reference LSF walls. The measured R -value ($1.752 \text{ m}^2\cdot\text{K}/\text{W}$) of the NLB reference LSF wall (Figure 7a) is slightly bigger (+2%) than the predicted THERM value ($1.719 \text{ m}^2\cdot\text{K}/\text{W}$). The LB reference LSF wall (Figure 7b) measured R -value ($1.558 \text{ m}^2\cdot\text{K}/\text{W}$) is slightly smaller (-2%) than the modelling result value ($1.594 \text{ m}^2\cdot\text{K}/\text{W}$). Thus, this accuracy range ($\pm 2\%$) was found to be a good agreement between predicted and simulated conductive R -values, given all the uncertainties involved within the simulations and measurements.

Moreover, it is well visible in the predicted temperature colour distribution (Figure 7) the thermal bridge effect due to the steel stud increased heat transfer, which significantly decrease the thermal resistance of the wall when compared with homogeneous layers simplified model without steel studs. This R -value decrease is $1.138 \text{ m}^2\cdot\text{K}/\text{W}$ (-40%) for the NLB LSF wall (Figure 7a) and $1.289 \text{ m}^2\cdot\text{K}/\text{W}$ (-45%) for the LB LSF wall (Figure 7b).

3. Results

3.1. Non-load-bearing LSF Walls

Table 4 display the conductive thermal resistances predicted by THERM software 2D FEM models and the measured values for non-load-bearing (NLB) walls, as well as the absolute and percentage differences between measured and predicted R -values. The results are organized into four groups: (1) the reference non-load-bearing R -value (NLB_{ref}), *i.e.*, for the LSF wall without any thermal break (TB) strip; (2) the LSF walls with an inner TB strip (NLB_{TBin}) made of different materials (R1, R0 and AG); (3) the LSF walls with an outer TB strip (NLB_{TBout}), and; (4) the LSF walls with two TB strips (NLB_{TBx2}), inner and outer.

The first remarkable feature is that measured R -values are quite similar to the predicted ones, being the differences ranging between $\pm 2\%$, ensuring the reliability of both measured and predicted R -values. As expected, the use of thermal break (TB) strips allow to increase the R -value of the LSF wall, given the heat loss reduction due to steel studs thermal bridges mitigation. Also as expected, this R -value increase depends mainly on the number of the TB strips and also on its material thermal conductivity.

For a better visualization and comparison, the measured R -values are graphically displayed in Figure 8. In this figure is displayed the R -value increase (in percentage), for each wall configuration, computed having as reference the non-load-bearing LSF wall ($1.752 \text{ m}^2 \cdot \text{K}/\text{W}$). As additional reference, the expected R -value rise due to an homogeneous mineral wool (MW) layer, within the wall cavity, with 10 mm (one TB strip) and 20 mm (two TB strips), is also displayed. This is justified by the enlarged thickness of the expansible MW inside the thicker insulation cavity due to the use of the TB strips in the outside stud flanges.

As expected, given the lower thermal conductivity of the MW ($0.035 \text{ W}/(\text{m} \cdot \text{K})$)

comparatively with the two TB strip materials, *i.e.*, Acousticork R1-recycled rubber (0.122 W/(m·K)) and R0-cork composite (0.088 W/(m·K)), the *R*-values increase for these LSF walls (ranging from +10% up to +14% for single TB strips and from +22% to +26% for double ones), are lower than +16% and +33% reference percentage values, respectively for single (10 mm thick) and double (20 mm thick) TB strips.

Table 4. Thermal resistances (surface-to-surface) predicted (THERM) and measured for non-load-bearing LSF walls.

Wall Code	Layer Description: outer to inner layers (thickness of the layer in mm)	R-value [m ² ·K/W]	
		THERM	Measured
NLB _{ref}	2GPB(12.5) + [C90+MW(90)] + 2GPB(12.5)*	1.719	1.752
	Difference: Absolute [m ² ·K/W] & Percentage [%]	+0.033	+2%
NLB _{R1in}	2GPB(12.5) + [C90+MW(90)+R1(10)] + 2GPB(12.5)	1.932	1.964
	Difference: Absolute [m ² ·K/W] & Percentage [%]	+0.032	+2%
NLB _{R0in}	2GPB(12.5) + [C90+MW(90)+R0(10)] + 2GPB(12.5)	2.006	2.006
	Difference: Absolute [m ² ·K/W] & Percentage [%]	+0.000	0%
NLB _{AGin}	2GPB(12.5) + [C90+MW(90)+AG(10)] + 2GPB(12.5)	2.359	2.404
	Difference: Absolute [m ² ·K/W] & Percentage [%]	+0.045	+2%
NLB _{R1out}	2GPB(12.5) + [R1(10)+C90+MW(90)] + 2GPB(12.5)	1.931	1.931
	Difference: Absolute [m ² ·K/W] & Percentage [%]	+0.000	0%
NLB _{R0out}	2GPB(12.5) + [R0(10)+C90+MW(90)] + 2GPB(12.5)	1.975	1.965
	Difference: Absolute [m ² ·K/W] & Percentage [%]	-0.010	-1%
NLB _{AGout}	2GPB(12.5) + [AG(10)+C90+MW(90)] + 2GPB(12.5)	2.358	2.414
	Difference: Absolute [m ² ·K/W] & Percentage [%]	+0.056	+2%
NLB _{R1x2}	2GPB(12.5) + [R1(10)+C90+MW(90)+R1(10)] + 2GPB(12.5)	2.147	2.142
	Difference: Absolute [m ² ·K/W] & Percentage [%]	-0.005	-0%
NLB _{R0x2}	2GPB(12.5) + [R0(10)+C90+MW(90)+R0(10)] + 2GPB(12.5)	2.236	2.202
	Difference: Absolute [m ² ·K/W] & Percentage [%]	-0.034	-2%
NLB _{AGx2}	2GPB(12.5) + [AG(10)+C90+MW(90)+AG(10)] + 2GPB(12.5)	2.892	2.885
	Difference: Absolute [m ² ·K/W] & Percentage [%]	-0.007	-0%

*Reference non-load-bearing (NLB) LSF wall; GPB – Gypsum plasterboard; C90 – Steel stud type and web dimension in mm; MW – Mineral wool; R1 – Acousticork (recycled rubber) thermal break strip; R0 – Acousticork (recycled rubber and cork) thermal break strip; AG – Aerogel thermal break strip.

Looking to the aerogel (AG) TB strips, given its lower thermal conductivity (0.015 W/(m·K)), the increase in the measured *R*-values (+37, +38% and 65%) are considerable greater than the above mentioned reference MW percentages, *i.e.*, +16% and 33% for single and double TB strips, respectively. Thus, these aerogel TB strips exhibit a significant better thermal performance than R1 and R0 TB strips, as well as than an equivalent MW homogeneous layer. Moreover, the thermal performance of the R0 (rubber and cork

composite) TB strip is only slightly better than the R1 (recycled rubber), which could be justified by their similar thermal conductivity values.

Notice that, there is only one evaluated TB strips configuration that is able to reach the *R*-value provided for a homogeneous wall without steel studs (2.857 m²·K/W), which is the two aerogel TB strips solution (2.885 m²·K/W), fully mitigating the steel frame thermal bridges effect.

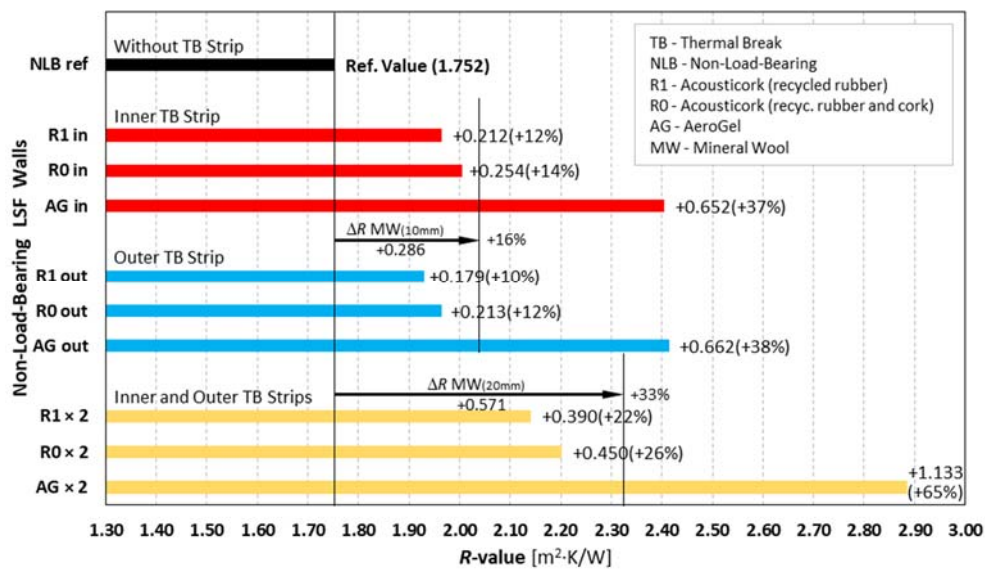


Figure 8. Measured thermal resistances for non-load-bearing (NLB) LSF walls.

After analysing the overall thermal performance improvement due to the use of TB strips, the related steel stud thermal bridge mitigation effect is assessed making use of infrared (IR) thermography. With this purpose, Figure 9 exhibit the infrared images of the tested non-load-bearing LSF walls (cold surface), while in Figure 10 are displayed the surface temperature profiles recorded along the horizontal lines (L1 to L4) positioned and identified in Figure 9 IR images. To an easier assessment and comparison between the four measured LSF walls, in Figure 9 the IR colour legend scale is the same for all the IR images presented.

Looking to the IR image of the LSF wall without any TB strip (Figure 9a) is very

well visible the presence of the central vertical steel stud, due to the higher surface temperature originated by the increased heat transmission across it. This steel thermal bridge effect is even more visible in Figure 10 (Line 1), where the maximum temperature identified in the stud vicinity was 11.7°C, while the average temperature between studs is quite lower (9.5°C). Notice that the two lateral vertical steel studs are not visible in these IR images due to its position within the mini hot/cold boxes experimental apparatus, *i.e.*, they are between the lateral vertical walls of the climatic chambers.

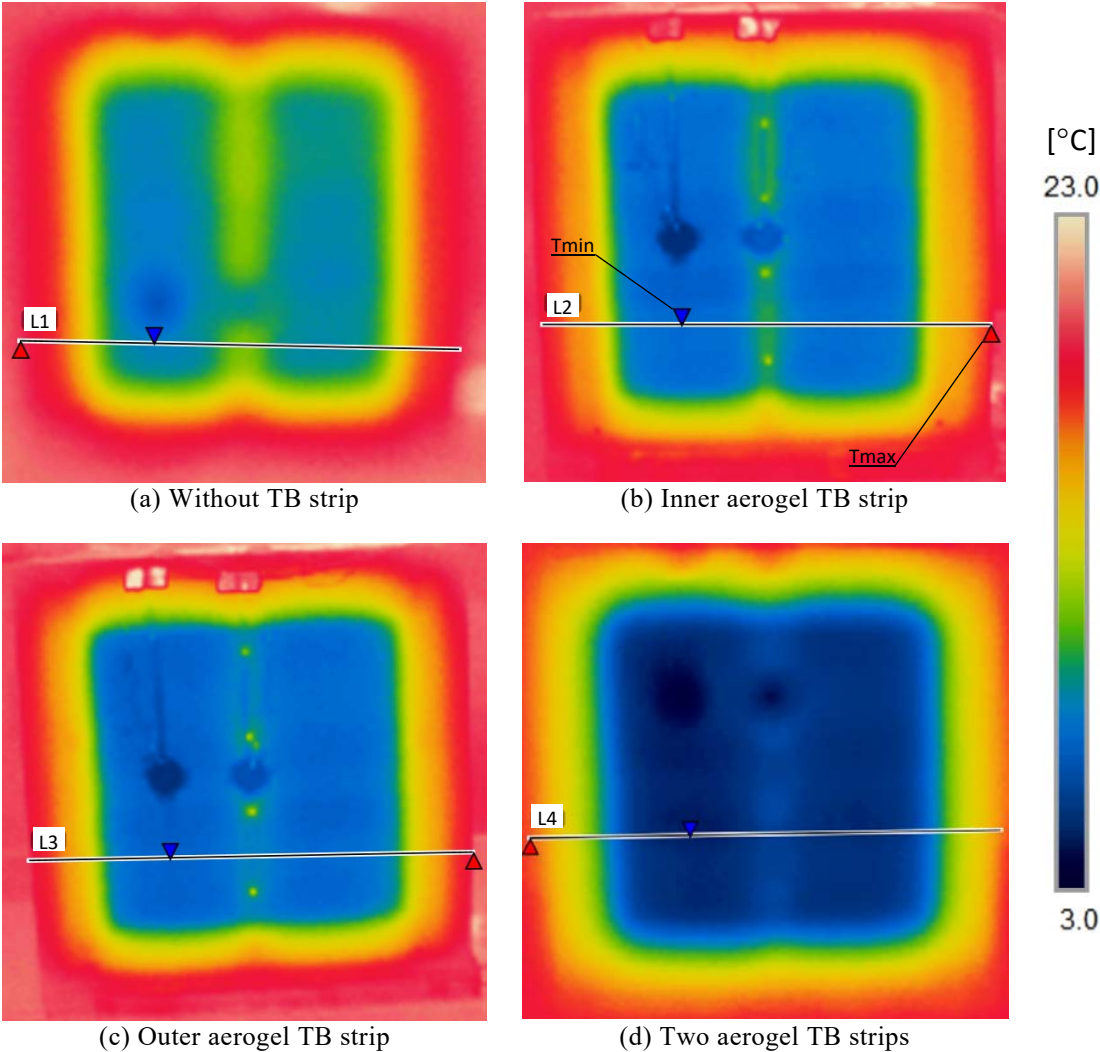


Figure 9. IR images of the assessed non-load-bearing LSF walls: Cold surface.

The other three images of Figure 9 (b to d) correspond to the LSF walls with aerogel TB strips applied in the inner flange (Figure 9b), outer flange (Figure 9c) and both inner and outer flanges (Figure 9d). Comparing these three images with the reference one without

any TB strip (Figure 9a), is quite well visible the lower steel stud thermal bridge effect (central vertical yellow line less visible), being this more evident for the outer (Figure 9c) and double aerogel TB strips (Figure 9d). Moreover, it is also well visible the significant overall thermal performance improvement, previously reported in Table 4 and Figure 8 (+65%), when are used two aerogel TB strips (Figure 9d), because the lower surface temperature (darker blue colour) in comparison with the other three LSF walls.

Looking to the horizontal lines surface temperature profiles (Figure 10), both lines L2 and L3 exhibits a similar temperature reduction, being the major difference at the central steel stud zone, where the outer TB strip originates a lower maximum temperature (8.9°C) in comparison with the inner TB strip (10.3°C). In accordance with previous related IR images (Figure 9), the line L4 for the LSF wall with two aerogel TB trips corroborate a significant better thermal performance, exhibiting a considerable lower maximum temperature at central steel stud (5.7°C) and also at the cavity insulation region with an average temperature equal to 4.9°C.

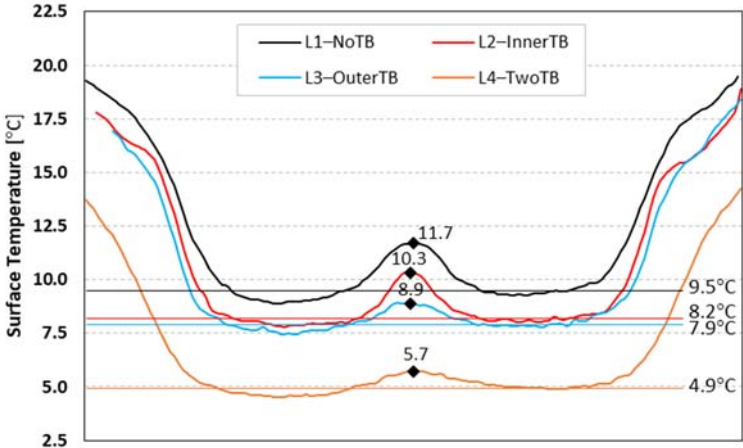


Figure 10. Horizontal temperature lines from IR images of the assessed non-load-bearing LSF walls, on the cold surface, with and without aerogel thermal breaks (TB).

3.2. Load-bearing LSF Walls

Table 5 display the obtained measured and predicted results for the load-bearing (LB) or structural LSF walls. Again, there is a good agreement between the measured *R*-

values and the predicted ones, ranging the differences between -1% and -3%.

Notice that, the reference R -value for the load-bearing LSF wall ($1.558 \text{ m}^2\cdot\text{K}/\text{W}$) is smaller than the previously presented (Table 5) non-load-bearing LSF wall reference R -value ($1.752 \text{ m}^2\cdot\text{K}/\text{W}$). This could be justified mainly by the greater steel studs thickness, 1.5 mm instead of 0.6 mm.

Again, it is well visible the R -value increase due to the use of TB strips along the steel stud flanges, being this increase greater for lower thermal conductivity materials (e.g. AG - aerogel) and when are used two TB strips.

Table 5. Thermal resistances (surface-to-surface) predicted (THERM) and measured for load-bearing LSF walls.

Wall Code	Layer Description: outer to inner layers (thickness of the layer in mm)	R-value [$\text{m}^2\cdot\text{K}/\text{W}$]	
		THERM	Measured
LB _{ref}	OSB(12) + [C90+MW(90)] + OSB(12)GPB(12.5)*	1.594	1.558
	Difference: Absolute [$\text{m}^2\cdot\text{K}/\text{W}$] & Percentage [%]	-0.036	-2%
LB _{R1in}	OSB(12) + [C90+MW(90)+R1(10)] + OSB(12)GPB(12.5)	1.806	1.747
	Difference: Absolute [$\text{m}^2\cdot\text{K}/\text{W}$] & Percentage [%]	-0.059	-3%
LB _{R0in}	OSB(12) + [C90+MW(90)+R0(10)] + OSB(12)GPB(12.5)	1.853	1.813
	Difference: Absolute [$\text{m}^2\cdot\text{K}/\text{W}$] & Percentage [%]	-0.040	-2%
LB _{AGin}	OSB(12) + [C90+MW(90)+AG(10)] + OSB(12)GPB(12.5)	2.246	2.198
	Difference: Absolute [$\text{m}^2\cdot\text{K}/\text{W}$] & Percentage [%]	-0.048	-2%
LB _{R1out}	OSB(12) + [R1(10)+C90+MW(90)] + OSB(12)GPB(12.5)	1.803	1.755
	Difference: Absolute [$\text{m}^2\cdot\text{K}/\text{W}$] & Percentage [%]	-0.048	-3%
LB _{R0out}	OSB(12) + [R0(10)+C90+MW(90)] + OSB(12)GPB(12.5)	1.875	1.826
	Difference: Absolute [$\text{m}^2\cdot\text{K}/\text{W}$] & Percentage [%]	-0.049	-3%
LB _{AGout}	OSB(12) + [AG(10)+C90+MW(90)] + OSB(12)GPB(12.5)	2.252	2.205
	Difference: Absolute [$\text{m}^2\cdot\text{K}/\text{W}$] & Percentage [%]	-0.047	-2%
LB _{R1x2}	OSB(12) + [R1(10)+C90+MW(90)+R1(10)] + OSB(12)GPB(12.5)	2.010	1.953
	Difference: Absolute [$\text{m}^2\cdot\text{K}/\text{W}$] & Percentage [%]	-0.057	-3%
LB _{R0x2}	OSB(12) + [R0(10)+C90+MW(90)+R0(10)] + OSB(12)GPB(12.5)	2.101	2.049
	Difference: Absolute [$\text{m}^2\cdot\text{K}/\text{W}$] & Percentage [%]	-0.052	-2%
LB _{AGx2}	OSB(12) + [AG(10)+C90+MW(90)+AG(10)] + OSB(12)GPB(12.5)	2.794	2.754
	Difference: Absolute [$\text{m}^2\cdot\text{K}/\text{W}$] & Percentage [%]	-0.040	-1%

*Reference load-bearing (LB) LSF wall; GPB – Gypsum plasterboard; C90 – Steel stud type and web dimension in mm; MW – Mineral wool; OSB – Oriented strand board; R1 – Acousticork (recycled rubber) thermal break strip; R0 – Acousticork (recycled rubber and cork) thermal break strip; AG – Aerogel thermal break strip.

Figure 11 displays the thermal performance improvement due to the use of TB strips on the load-bearing LSF walls, ranging the R -value increase from +12% (for inner R1

recycled rubber) up to +77% (for two aerogel TB strips). Again, the inner and outer TB strips performances are very similar, being in this case slightly better when located in the outer steel flange (+1%).

As for the non-load-bearing LSF walls, the major *R*-value increase occurred when are used two TB strips at both flanges (×2) and when the material of the TB strip has lower thermal conductivity, *i.e.*, aerogel (AG). In fact, the aerogel TB strips showed a significant increase in the measured *R*-values: +41% and +42% for inner and outer strips, respectively, and; +77% for double strips. Nevertheless, not even this best thermal performance configuration, with two aerogel TB strips (2.754 m²·K/W), is able to reach the *R*-value ensured by a homogeneous wall without steel studs (2.883 m²·K/W).

Comparing now these measurement results for the structural (Figure 11) with the non-structural LSF walls (Figure 8), both graphs exhibits the same trend, being the *R*-values greater for the non-structural LSF walls (Figure 8), as previously noticed and justified. However, the percentage increase in the *R*-values due to the use of TB strips is, in general, slightly higher in the load-bearing LSF walls (Figure 11), but not in absolute values (m²·K/W).

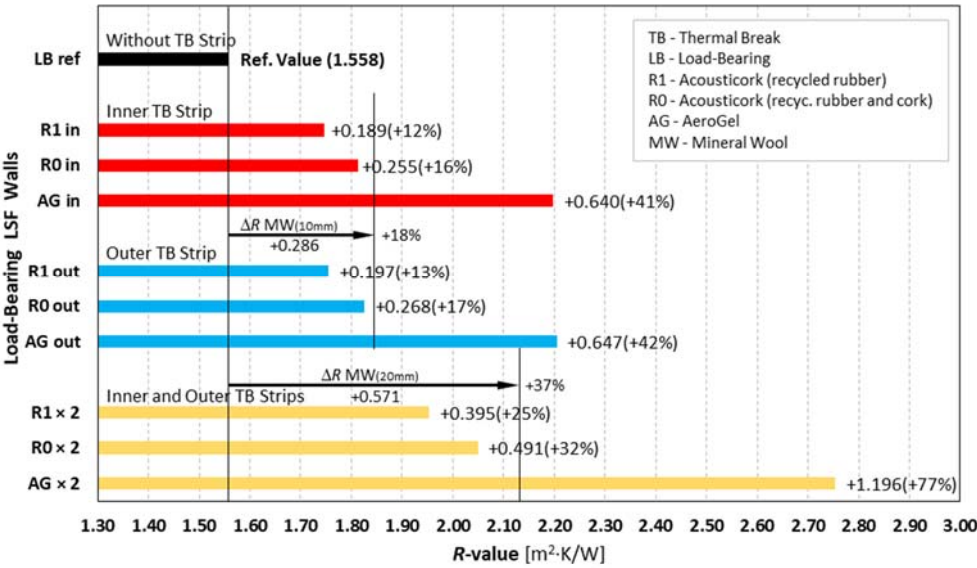


Figure 11. Measured thermal resistances for load-bearing (LB) LSF walls.

The IR images of the tested load-bearing LSF walls (cold surface) are displayed in Figure 12, while Figure 13 exhibits the surface temperature profiles recorded along the horizontal lines (L1 to L4) identified in Figure 12, for each one of the four LSF walls. Again the thermal bridge effect due to the central vertical steel stud is well visible, mainly when there is no TB strip (Figure 12a). This effect is attenuated due to use of aerogel TB strips, being majorly attenuated, in these images, for the outer (Figure 12c) and double TB strips (Figure 12d). This feature could be confirmed in Figure 13, where the temperature peak (increase) in the vicinity of the central steel stud is lower in both lines: L3 (outer TB strip) and L4 (double TB strips).

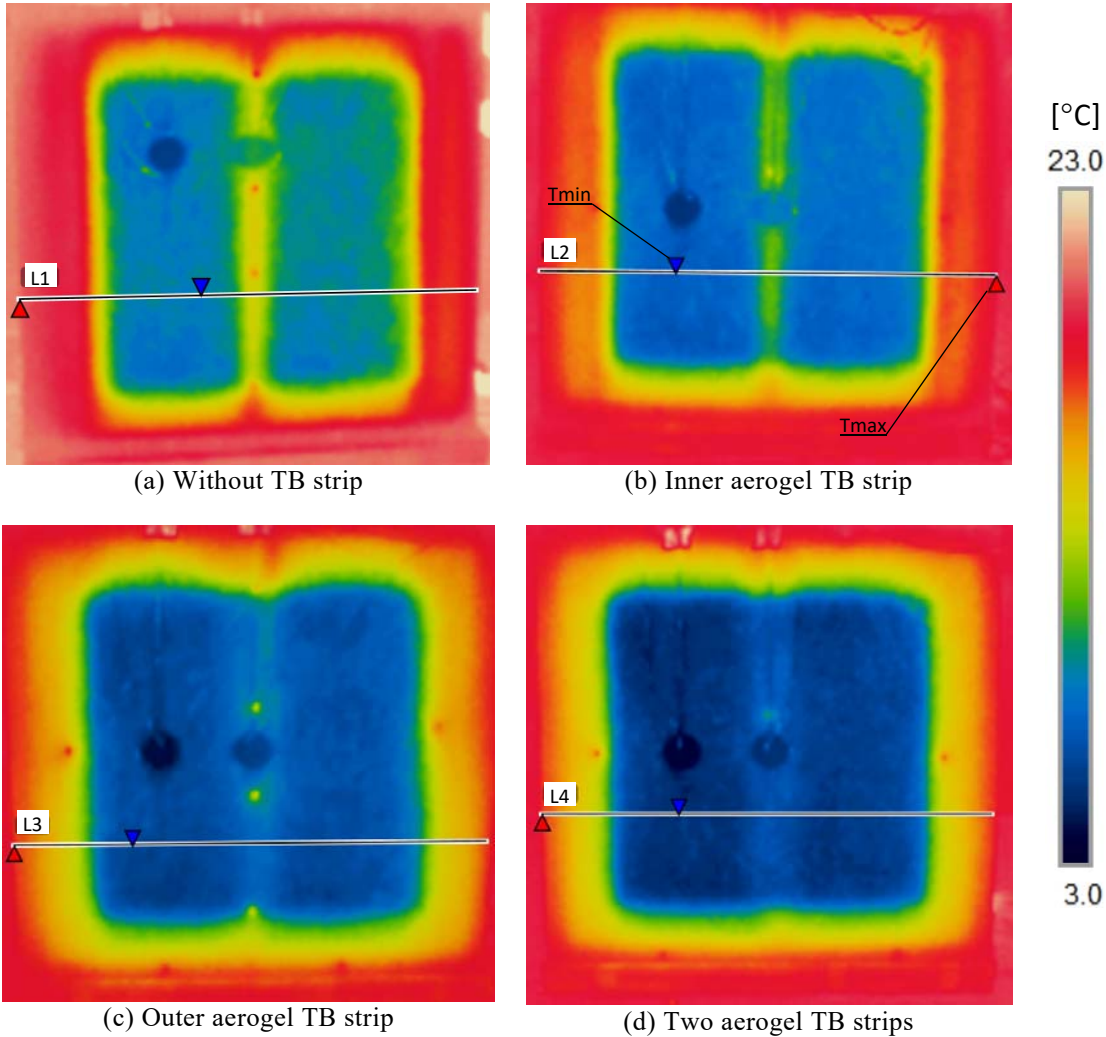


Figure 12. IR images of the assessed load-bearing LSF walls: Cold surface.

Comparing these surface temperature profiles (Figure 13) with the previous ones for the non-load-bearing LSF walls (Figure 10), it is noticed that the central peak temperatures are higher now for these load-bearing LSF walls, ranging from 7.0°C to 13.9°C, instead of the previous range, from 5.7°C up to 11.7°C. This confirms the higher steel stud thermal bridge effect and consequent worst thermal performance of the load-bearing LSF walls, as previously noticed. The reasonable for this, could be, as mentioned before, in the thicker steel studs (1.5 mm instead of 0.6 mm).

Another interesting feature, visible in Figure 13, is that the use of outer TB strips (L3) has a better thermal performance than inner TB strips (L2), given the lower surface temperatures and consequent lower heat flow crossing the LSF wall. This feature was previously mentioned and pointed out during the analysis of the results displayed in Figure 11, but this trend was not so evident (only 1% difference).

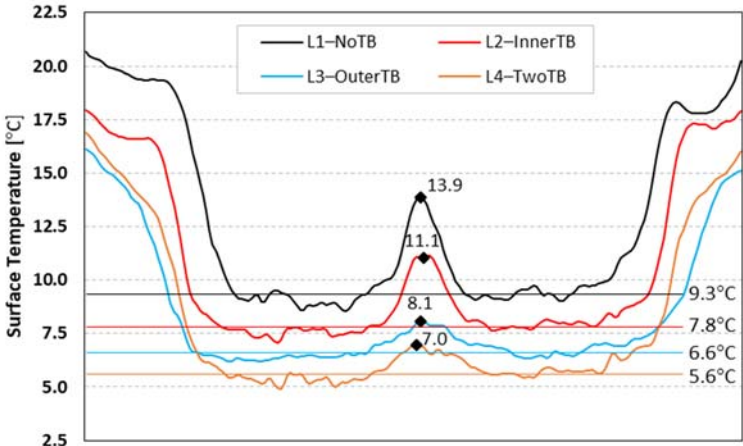


Figure 13. Horizontal temperature lines from IR images of the assessed load-bearing LSF walls, on the cold surface, with and without aerogel thermal breaks (TB).

4. Discussion

To allow an easier overall performance comparison, Figure 14 displays a graphical overview of the results previously presented for load- and non-load-bearing LSF walls, regarding the thermal resistance improvement provided by the TB strips.

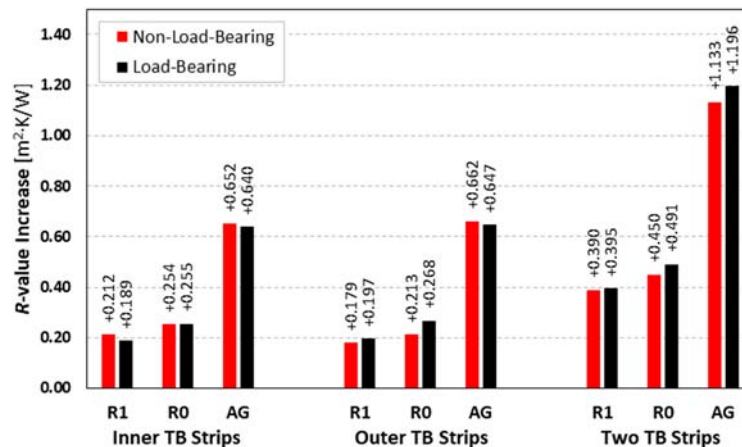


Figure 14. Thermal resistance increase due to thermal break (TB) strips use in load- and non-load-bearing LSF walls.

Comparing the thermal resistance improvement for load- and non-load-bearing LSF walls, it can be concluded that the TB strips are slightly more efficient in LB walls, mainly when applied in the outer or in both stud flanges. This feature could be related with the thicker steel studs in LB walls (1.5 mm instead of 0.6 mm). Moreover, the thermal performance improvement of aerogel (AG) TB strips is very significant, *i.e.*, around three times greater than recycled rubber (R1). Additionally, the R -value increase for the rubber/cork composite (R0) TB strips is only slightly higher (about +20%) than recycled rubber (R1).

In a previous study, Santos *et al.* [6] performed a parametric study, where the use of thermal break strips was also simulated. Even existing several differences between the present wall configurations and the former LSF walls (*e.g.*, the studs spacing was 600 mm, while here is 400 mm), some results comparisons are made next. These comparisons are made only for the non-load-bearing (NLB) walls, since the former load-bearing LSF facade

walls have ETICS (external thermal insulation composite system), which significantly change their thermal behaviour, *e.g.*, the former conductive R -value is much bigger ($3.453 \text{ m}^2\cdot\text{K}/\text{W}$) than here in this study ($1.558 \text{ m}^2\cdot\text{K}/\text{W}$).

Given the higher frequency of steel studs (400 mm) the reference surface-to-surface R -value here ($1.752 \text{ m}^2\cdot\text{K}/\text{W}$) is smaller than in the previous research work [6] ($1.967 \text{ m}^2\cdot\text{K}/\text{W}$), where the studs are spaced 600 mm apart. Comparing the thermal resistance improvement for the NLB walls when using aerogel inner TB strips, here in this study; $+0.652 \text{ m}^2\cdot\text{K}/\text{W}$ (+37%) (see Figure 8) with the previous study [6]; $+0.447 \text{ m}^2\cdot\text{K}/\text{W}$ (+23%), it can be concluded that the aerogel TB strips are much more effective in the present LSF wall configuration. This is due to the higher amount of steel when the vertical studs are spaced 400 mm (here in this study), instead of 600 mm (in ref. [6]), which leads to an higher importance of the thermal bridge effect due to the higher thermal conductivity of steel, increasing this way the effectiveness of TB strips.

5. Conclusions

In this work the thermal performance of thermal break (TB) strips in lightweight steel frame (LSF) partition walls was assessed making use of experimental lab measurements. Load- and non-load-bearing LSF walls were evaluated. Inner, outer and double TB strips were tested and three TB strip materials were evaluated: R1 – recycled rubber; R0 – rubber and cork composite, and; AG – aerogel.

The main conclusions of this research work could be summarized as follows:

- The inner and outer TB strips have very similar thermal performances. However, the outer TB strips appear to have slightly better performance in load-bearing LSF walls.
- As expected, the double TB strips have a significant thermal performance increase, when compared with single TB strips.
- The best performance TB material was the aerogel (AG), with a substantial improvement in comparison with the other two materials (R1 – Recycled rubber, and R0 – Rubber and cork composite).
- The R1 (recycled rubber) and R0 (rubber and cork composite) TB strips have a quite similar thermal performance.
- Only the two aerogel TB strips configuration, for a non-structural LSF wall, was able to reach the R -value provided for a homogeneous wall without steel studs, allowing to fully mitigate the steel frame thermal bridges effect.
- The thermal performance improvement due to the TB strips is identical for load-bearing and non-load-bearing LSF walls when looking to the absolute R -values increase, appearing to be slightly more effective in load-bearing LSF walls.

Another interesting concluding remark is that the used experimental lab apparatus, based in the standard heat flow meter (HFM) method [9], improved by using two heat flux sensors (one on each side of the wall sample), as suggested by Rasooli and Itard [22],

allowed to significantly reduce the expected uncertainty range indicated by ISO 9869-1 [9] for the HFM method *in situ* measurements [14%; 28%]. In fact, all the obtained measurement results were compared with the predictions provided by numerical 2D FEM models, exhibiting very good *R*-value agreements ($\pm 3\%$ error range) for the twenty assessed LSF walls, ensuring high robustness and reliability of the implemented measurement apparatus and test procedures.

This study allows to better understand and quantify the usefulness of thermal break strips in the increase of thermal resistance of load- and non-load-bearing walls, making use of three different materials and comparing three different stud flange positions (inner, outer and on both sides), which until now were not available in the literature. Moreover, the measured surface-to-surface *R*-values could be used as a benchmark for the validation of numerical simulations in LSF walls with similar configurations.

Funding

This research was funded by FEDER funds through the Competitvity Factors Operational Programme – COMPETE and by national funds through FCT – Foundation for Science and Technology, within the scope of the project POCI-01-0145-FEDER-032061.

Cofinanciado por: POCI-01-0145-FEDER-032061



UNIÃO EUROPEIA
Fundo Europeu
de Desenvolvimento Regional



Acknowledgments

The authors also want to thank the support provided by the following companies: Pertecno, Gyptec Ibéria, Volcalis, Sotinco, Kronospan, Hulkseflux, Hilti and Metabo.

References

- [1] N. Soares, P. Santos, H. Gervásio, J. J. Costa, and L. Simões da Silva, “Energy efficiency and thermal performance of lightweight steel-framed (LSF) construction: A review,” *Renew. Sustain. Energy Rev.*, vol. 78, pp. 194–209, 2017.
- [2] Morrison Hershfield, “Appendix B - Catalogue Thermal Data Sheets,” *Building Envelope Thermal Bridging Guide*, 2018. [Online]. Available: <https://www.bchydro.com/content/dam/BCHydro/customer-portal/documents/power-smart/builders-developers/appendix-b-full-version.pdf>. [Accessed: 06-May-2020].
- [3] C. Santos and L. Matias, *ITE50 - Coeficientes de Transmissão Térmica de Elementos da Envolvente dos Edifícios (in Portuguese)*. LNEC - Laboratório Nacional de Engenharia Civil, 2006.
- [4] P. Santos, G. Lemes, and D. Mateus, “Analytical Methods to Estimate the Thermal Transmittance of LSF Walls : Calculation Procedures Review and Accuracy Comparison,” *Energies*, vol. 13, no. 4, p. 840, 2020.
- [5] ISO 6946, “Building components and building elements — Thermal resistance and thermal transmittance - Calculation methods.” International Organization for Standardization, Geneva, Switzerland, 2017.
- [6] P. Santos, G. Lemes, and D. Mateus, “Thermal Transmittance of Internal Partition and External Facade LSF Walls: A Parametric Study,” *Energies*, vol. 12, no. 14, p. 2671, 2019.
- [7] ISO 10211, “Thermal bridges in building construction — Heat flows and surface temperatures - Detailed calculations.” ISO - International Organization for Standardization, Geneva, Switzerland, 2017.
- [8] N. Soares, C. Martins, M. Gonçalves, P. Santos, L. Simões da Silva, and J. J. Costa, “Laboratory and in-situ non-destructive methods to evaluate the thermal transmittance

- and behaviour of walls, windows, and construction elements with innovative materials: a review,” *Energy Build.*, vol. 182, pp. 88–110, 2019.
- [9] ISO 9869-1, “Thermal insulation – Building elements - In-situ measurement of thermal resistance and thermal transmittance. Part 1: Heat flow meter method.” ISO - International Organization for Standardization, Geneva, Switzerland, 2014.
- [10] J. Kosny, J. E. Christian, E. Barbour, and J. Goodrow, “Thermal performance of steel-framed walls,” ONRL report, Oak Ridge National Laboratory, USA, 1994.
- [11] M. Gorgolewski, “Developing a simplified method of calculating U-values in light steel framing,” *Build. Environ.*, vol. 42, no. 1, pp. 230–236, Jan. 2007.
- [12] ASHRAE, *Handbook of Fundamentals (SI Edition)*. ASHRAE - American Society of Heating, Refrigerating and Air-conditioning Engineers, Atlanta, USA, 2017.
- [13] E. Roque and P. Santos, “The Effectiveness of Thermal Insulation in Lightweight Steel-Framed Walls with Respect to Its Position,” *Buildings*, vol. 7(1), no. 13, pp. 1–18, 2017.
- [14] P. Santos, C. Martins, L. Simões da Silva, and L. Bragança, “Thermal performance of lightweight steel framed wall: The importance of flanking thermal losses,” *J. Build. Phys.*, vol. 38, no. 1, pp. 81–98, Jul. 2014.
- [15] C. Martins, P. Santos, and L. Simões da Silva, “Lightweight steel-framed thermal bridges mitigation strategies: A parametric study,” *J. Build. Phys.*, vol. 39, no. 4, pp. 342–372, 2016.
- [16] ISO 8301, “Thermal insulation – Determination of steady-state thermal resistance and related properties – Heat flow meter apparatus.” ISO - International Organization for Standardization, Geneva, Switzerland, 1991.
- [17] ASTM-C1046–95(Reapproved-2013), “Standard practice for in-situ measurement of heat flux and temperature on building envelope components.” ASTM - American

- Society for Testing and Materials, Philadelphia, USA, 2013.
- [18] ASTM-C1155–95(Reapproved-2013), “Standard practice for determining thermal resistance of building envelope components from the in-situ data.” ASTM - American Society for Testing and Materials, Philadelphia, USA, 2013.
- [19] ISO 8302, “Thermal insulation – Determination of steady-state thermal resistance and related properties – Guarded hot plate apparatus.” ISO - International Organization for Standardization, Geneva, Switzerland, 1991.
- [20] ISO 8990, “Thermal insulation - Determination of steady-state thermal transmission properties - Calibrated and guarded hot box.” ISO - International Organization for Standardization, Geneva, Switzerland, 1994.
- [21] ISO 9869-2, “Thermal insulation – Building elements - In-situ measurement of thermal resistance and thermal transmittance. Part 2: Infrared method for frame structure dwelling.” ISO - International Organization for Standardization, Geneva, Switzerland, 2018.
- [22] A. Rasooli and L. Itard, “In-situ characterization of walls’ thermal resistance: An extension to the ISO 9869 standard method,” *Energy Build.*, vol. 179, pp. 374–383, 2018.
- [23] K. Gaspar, M. Casals, and M. Gangoells, “Review of criteria for determining HFM minimum test duration,” *Energy Build.*, vol. 176, pp. 360–370, 2018.
- [24] G. Ficco, F. Iannetta, E. Ianniello, F. R. D’Ambrosio Alfano, and M. Dell’Isola, “U-value in situ measurement for energy diagnosis of existing buildings,” *Energy Build.*, vol. 104, pp. 108–121, 2015.
- [25] D. S. Choi and M. J. Ko, “Comparison of various analysis methods based on heat flowmeters and infrared thermography measurements for the evaluation of the in situ thermal transmittance of opaque exterior walls,” *Energies*, vol. 10, no. 7, 2017.

- [26] P. Santos, G. Lemes, and D. Mateus, “Analytical Methods to Estimate the Thermal Transmittance of LSF Walls: Calculation Procedures Review and Accuracy Comparison,” *Energies*, vol. 13, no. 4, p. 840, 2020.
- [27] P. Santos, M. Gonçalves, C. Martins, N. Soares, and J. J. Costa, “Thermal Transmittance of Lightweight Steel Framed Walls: Experimental Versus Numerical and Analytical Approaches,” *J. Build. Eng.*, vol. 25, no. April, p. 100776, 2019.
- [28] I. A. Atsonios, I. D. Mandilaras, D. A. Kontogeorgos, and M. A. Founti, “Two new methods for the in-situ measurement of the overall thermal transmittance of cold frame lightweight steel-framed walls,” *Energy Build.*, vol. 170, pp. 183–194, 2018.
- [29] T. Höglund and H. Burstrandb, “Slotted steel studs to reduce thermal bridges in insulated walls,” *Thin-Walled Struct.*, vol. 32, pp. 81–109, 1998.
- [30] Tyre4BuildIns, “Research project Tyre4BuildIns - ‘Recycled tyre rubber resin-bonded for building insulation systems towards energy efficiency’, funded by FEDER European and FCT National funds. Reference: POCI-01-0145-FEDER-032061. University of Coimbra, PT,” 2020. [Online]. Available: www.tyre4buildins.dec.uc.pt. [Accessed: 15-Jan-2020].
- [31] MS-R0 Test Report, “Test report Ref. 5015 PE 1977/08 - Determination of Thermal Conductivity (Acousticork MS-R0).” Departamento de Engenharia Têxtil, Universidade do Minho, 2008.